Palaeoenvironmental variability and carbon cycle perturbations during the Smithian-Spathian (Early Triassic) in Central Spitsbergen

Blattmann, Franziska R ; Schneebeli-Hermann, Elke ; Adatte, Thierry ; Bucher, Hugo F R ; Vérard, Christian ; Hammer, Øyvind ; Luz, Zoneibe A S ; Vennemann, Torsten W

DOI: https://doi.org/10.18261/let.57.2.1

Lethaia
AN INTERNATIONAL JOURNAL OF PALAEONTOLOGY AND STRATIGRAPHY

Palaeoenvironmental variability and carbon cycle perturbations during the Smithian-Spathian (Early Triassic) in Central Spitsbergen

FRANZISKA R. BLATTMANN, ELKE SCHNEEBELI-HERMANN, THIERRY ADATTE, HUGO F.R. BUCHER, CHRISTIAN VÉRARD, ØYVIND HAMMER, ZONEIBE A.S. LUZ AND TORSTEN W. VENNEMANN

LETHAIA

The Early Triassic Smithian and Spathian time intervals are characterized by perturbations in the global carbon cycle, fluctuations in sea surface temperature, high turnover rates of marine nekton, and a change in terrestrial vegetation. Despite the importance of this time interval, comprehensive multiproxy investigations from Early Triassic high and middle latitude regions remain scarce due to the difficulty in accessing sections. The objective of this study is to increase our understanding of regional and local palaeoenvironmental and carbon cycle perturbations from a middle Smithian to late Spathian middle latitude section from Central Spitsbergen. Geochemical analyses show an increase in phosphorus and nitrogen just at and above the Smithian–Spathian boundary (SSB). High primary productivity led to increasingly anoxic conditions in bottom waters during the middle and late Spathian, enhancing the preservation of organic matter in the sediments. Anoxic conditions restrain phosphorus remineralization, allowing it to be recycled within the water column. This increase in anoxia is consistent with observations in other Arctic basins, demonstrating larger regional similarities in palaeoenvironmental conditions. The fluctuations in isostatic and eustatic sea levels affected organic carbon sequestration by regulating organic matter mineral interactions via the control of grain size within the sediment. This study demonstrates that local organic carbon sequestration in the Barents Sea shelf during the Spathian was influenced by a multitude of factors, including sedimentology, redox conditions, nutrient availability, and primary productivity. □ *Vikinghøgda Formation, bulk rock geochemistry, particulate organic matter, extinction recovery, carbon isotopes, Stensiöfjellet*

Franziska R. Blattmann ✉ [Franziska.Blattmann@unil.ch], Zoneibe A.S. Luz [zoneibe.luz@gmail.com] and Torsten W. Vennemann [Torsten.Vennemann@unil.ch], Institute of Earth Surface Dynamics, University of Lausanne, Quartier UNIL-Mouline, 1015 Lausanne, Switzerland; Elke Schneebeli-Hermann [elke.schneebeli@pim.uzh.ch] and Hugo F.R. Bucher [bucherhugo9@pim.uzh.ch], Department of Palaeontology, University of Zürich, Karl-Schmid-Strasse 4, 8006 Zürich, Switzerland; Thierry Adatte [Thierry.Adatte@unil.ch], Institute of Earth Sciences, University of Lausanne, Quartier UNIL-Mouline, CH-1015 Lausanne, Switzerland; Christian Vérard [Christian.Verard@unige.ch], Section of Earth and Environmental Sciences, University of Geneva, Rue des Maraîchers 13, CH-1205 Geneva, Switzerland; Øyvind Hammer [oyvind.hammer@nhm.uio.no], Natural History Museum, University of Oslo, Pb. 1172 Blindern, 0318 Oslo, Norway; *manuscript received on 08/08/2023; manuscript accepted on 02/02/2024; manuscript published on 20/06/2024 in* Lethaia 57(2).

The Early Triassic is marked by diverging biodiversity patterns and large fluctuations in carbon isotope ($\delta^{13}C$) composition (Brayard & Bucher 2015; Grasby *et al.* 2016b; Hautmann *et al.* 2015; Meyer *et al.* 2011; Payne *et al.* 2004). The Smithian was a time interval of intense carbon cycle instability, spore-dominated flora, a thermal climate maximum and a prolonged negative $\delta^{13}C$ excursion (e.g. Goudemand *et al.* 2019; Hermann *et al.* 2011a; Payne *et al.* 2004; Widmann *et al.* 2020; Zhang *et al.* 2019). The late Smithian marks the onset of a global positive $\delta^{13}C$ excursion, which peaks at the Smithian-Spathian boundary (SSB) (Galfetti *et al.* 2007; Romano *et al.* 2013). The SSB definition used here follows Brühwiler *et al.* (2010) and is based on ammonoid zones. We are aware that there is no official definition of the SSB and other definitions exists (e.g. Zhang *et al.* 2019). The origin of this global positive $\delta^{13}C_{org}$ excursion is attributed to global carbon sequestration (Widmann *et al.* 2020). The onset of the positive $\delta^{13}C$ excursion in the latest Smithian coincides with the extinction of marine nektonic organisms (Brayard & Bucher 2015; Orchard 2007; Stanley 2009), the beginning of a gymnosperm recovery (Hermann *et al.* 2011b), a global cooling trend (Goudemand *et al.* 2019; Luz 2022) and an eustatic sea-level decrease (Embry 1997).

https://doi.org/10.18261/let.57.2.1

This study presents a detailed multiproxy approach investigating the redox condition, nutrient cycling, sedimentology, and sea level fluctuations to better constrain factors influencing organic carbon burial across the Smithian and Spathian substages. Constraining factors influencing local organic carbon burial is a central aspect in gaining a better understanding of the local carbon cycle perturbation. The studied Smithian and Spathian sedimentary succession is the Stensiöfjellet section in Central Spitsbergen, which represents the transition between shelf and open marine depositional environments of the Panthalassa Ocean.

Geological Setting

The Lower Triassic sedimentary deposits of the Svalbard archipelago in Arctic Norway are part of the Sassendalen Group. In western Spitsbergen, the Lower Triassic part of the Sassendalen Group is divided into the Vardebukta and Tvillingodden formations. In central and eastern Spitsbergen as well as on Edgeøya the Lower Triassic part of the Sassendalen Group consists of the Vikinghøgda Formation. Across Svalbard a consistent eastward-deepening trend can be noted for these Lower Triassic deposits (Mørk *et al.* 1982). The depositional environment is thought to be a gently sloping marine ramp deepening stepwise during the Early to Middle Triassic (Mørk *et al.* 1999; Wignall *et al.* 2016). The Vikinghøgda Formation of central Spitsbergen is, therefore, the distal continuation of the shallow marine deposits of the Vardebukta and Tvillingodden Formations of western Spitsbergen. It is subdivided into the Deltadalen, Lusitaniadalen and Vendomdalen members. In central Spitsbergen the Vikinghøgda Formation is approximately 250 metres thick (Mørk *et al.* 1999).

The Stensiöfjellet study site is located in central Spitsbergen, on the north side of the Sassendalen valley (Lat = 78.283058°N; Long = 17.716164°E) (Fig. 1). The Lusitaniadalen and Vendomdalen members outcropping at Stensiöfjellet are equivalent to the Tvillingodden Formation of western Spitsbergen. The lithology of these members consists of sandy silts grading into silty shales and black shales. Horizons of calcareous nodules are found in both members (Hammer *et al.* 2019). A hiatus is present throughout all of Svalbard at the Lusitaniadalen and Vendomdalen Member boundary and corresponds approximately to the SSB (Mørk *et al.* 1999; Vigran *et al.* 2014). The Stensiöfjellet section encompasses the upper part of the middle Smithian and the entire Spathian substages and is dated in Hansen *et al.* (2021), Hansen *et al.* (2024) and Leu *et al.* (2024) (Fig. 2).

Methods

The succession at Stensiöfjellet has been sampled for fossils, shales, and carbonates, and analysed for their geochemistry and palynology. In this paper the

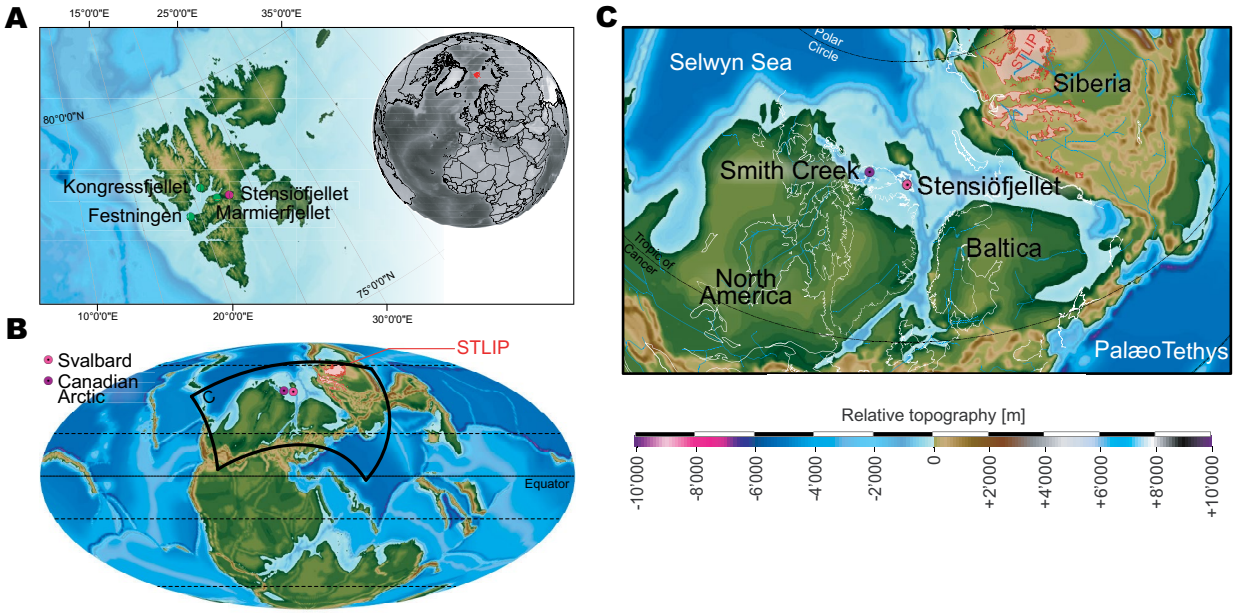

Fig. 1. A. map of Svalbard showing sections mentioned throughout the manuscript. B, palaeogeographical reconstruction of Pangaea during the Early Triassic (Vérard 2019). C. Close-up of northern middle and high latitudes with labelled sites.

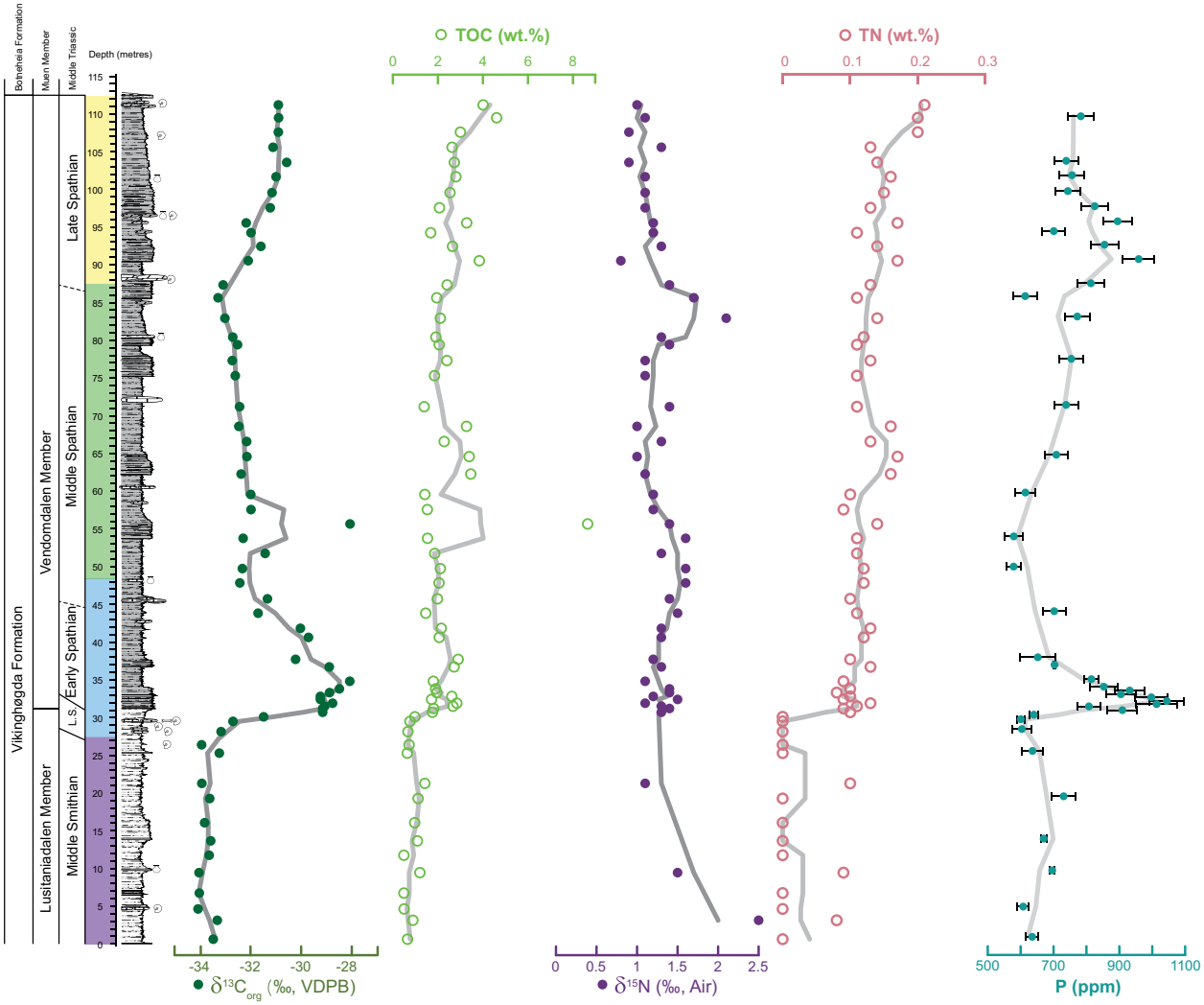

Fig. 2. The Stensiöfjellet section with formation, member boundaries and Lower Triassic substages following the biostratigraphy of Hansen *et al.* (2021, 2024) and Leu *et al.* (2024). The colour code across the depth scale bar is also used in Figure 4. The $\delta^{13}C_{org, bulk}$, total organic carbon (TOC, wt. %), $\delta^{15}N$, total nitrogen (TN, wt. %) and total phosphorus (P) data are plotted against depth of the section. The grey line in each diagram represents a 3-point moving average.

Stensiöfjellet A (STA) section has been analysed and is referred to as just Stensiöfjellet throughout the text. For fossil (e.g. Leu *et al.* 2024) related research Stensiöfjellet C (STC) was sampled roughly 500 m to the northeast.

Sedimentology and mineralogy

Thin sections of the shale and carbonate intervals were made at the University of Lausanne for microfacies analysis. A Keyence VHX-7000 microscope was used to make images.

The bulk and clay mineralogical composition were determined with X-ray powder diffraction (XRD) using a Thermo Scientific ARL X-TRA Diffractometer. Samples were crushed and milled with an agate mortar and pestle to a grain size <125 μm for bulk rock analysis. The clay mineralogical samples were not milled, but gently crushed with a hydraulic press and prepared according to the protocol of Kübler (1983). A semi-quantification was done using external standards following Adatte *et al.* (1996) and Kübler (1983).

Organic geochemistry and palynology

Organic matter was quantified and characterized at the University of Lausanne on powdered whole rocks using a Rock-Eval 6. Samples were pulverized using a handheld drill. The IFP 160000 standard was used to calibrate all measurements with an instrumental precision of 2% (Espitalie *et al.* 1986).

For the analysis of particulate organic matter, sixty-one samples were cleaned, crushed and weighed

(15 g on average) and subsequently treated with concentrated hydrochloric and hydrofluoric acid as described by Traverse (2007). The residues were sieved over a 11-µm mesh screen. For palynofacies analysis organic matter particles were counted on unoxidized slides to a minimum of 250 counts. Particle counts included the categories of translucent and opaque phytoclasts (charcoal), but also degraded terrestrial organic matter (pseudoamorphous particles, some with angular shape and/or remaining internal structure). Cuticles, inertinite, membranes, spores and bisaccate pollen grains, and fungal remains (sensu Hochuli *et al.* 1989) were also counted (Batten *et al.* 1996; Tyson 1995). Aquatic particles include homogenized sheets and flakes (sensu Vigran in Mørk *et al.* 1999), acritarchs (*Micrhystridium* spp. and *Veryhachium* spp.), *Leiospheridia* spp., *Tasmanites* spp., algal clusters (comparable to the algal colonies described by Vigran in Mørk *et al.* (1999)), amorphous organic matter, and foraminiferal test linings.

Slides are stored in the repository of the Palaeontological Institute and Museum, University of Zurich, and are found under PIMUZ A/VI 162 to PIMUZ A/VI 166.

Elemental composition

Element concentrations were measured on shales. The bulk rock elemental composition was determined with both X-ray fluorescence (XRF) spectrometry and inductively coupled plasma optical emission spectrometry (ICP-OES) for cross comparison. A Philips PW2400 XRF spectrometer was used with Rh-Kα radiation and a power of 2400 W. The reproducibility varies between 0.5 and 5% depending on the element. The accuracy was assessed by means of standard reference materials (NIM-G; SDC; BHVO; QLO). For the ICP-OES measurements an aqua regia (1:3 v:v 15 M HNO_3/12 M HCl) extraction was done for 2 hours at 110 °C. The extraction was measured using a Perkin-Elmer Optima 8300. The Chemical Index of Alteration (CIA) was calculated from ICP-OES data and corrected for carbonate content following McLennan (1993):

$$CIA = Al_2O_3 \times 100/ (Al_2O_3 + Na_2O^* + Na_2O + K_2O) \quad (1)$$

Phosphorus was extracted by $MgNO_3$ oxidation at 550 °C for 3 hours following the Aspila *et al.* (1976) method. The P concentration was measured on three analytical replicates using the phosphomolybdate blue method with a TECAN SPARK multimode microplate reader (Nagul *et al.* 2015). Total nitrogen was measured with a Thermo Finnigan Flash EA 1112 at 900 °C. Analytical precision and accuracy were determined by replicate analyses and by comparison with an organic analytical standard composed of Cystine and are better than 0.1% (1σ) nitrogen determinations.

Carbon and nitrogen isotopes

Bulk $\delta^{13}C_{carb}$ and $\delta^{18}O$ values were measured on shales using a Gasbench II connected to a Finnigan Delta Plus XL mass spectrometer according to the method of Spötl & Vennemann (2003). The samples were run at 70 °C with 100% orthophosphoric acid to measure the isotopic composition of all carbonate phases on CO_2. All measurements were calibrated against the Carrara Marble in-house standard, normalized to the VPDB-scale with NBS-19.

$\delta^{13}C_{org}$ and $\delta^{15}N$ values were measured on decarbonated samples. Samples were decarbonated using 3 M HCl. After the residues were rinsed several times with deionized water and dried in an oven at 45 °C, the isotope compositions were measured with a Carlo Erba (CE 1100) elemental analyser (EA) linked to a ThermoFisher Delta V mass spectrometer. Samples were reacted at 1050 °C in a stream of He-carrier gas spiked with oxygen gas. External reproducibility of internal standards (glycine, pyridine, urea, graphite, nitrate) was better than 0.15‰ and samples were calibrated against IAEA standards (USGS-24 graphite, NBS-22 oil).

Results

Sedimentology and mineralogy

The Stensiöfjellet section encompasses the upper part of the Lusitaniadalen Member and the complete Vendomdalen Member of the Vikinghøgda Formation. The boundary between the Lusitaniadalen and Vendomdalen members is marked by a yellow-weathering dolomitic bed (Fig. 3A).

The Lusitaniadalen Member consists of a light sandy shale, with a finely laminated texture containing non-recognizable microfossil material in thin sections (Fig. 3B). Intercalated carbonate nodule beds contain ammonoids and bivalves (Hansen *et al.* 2021; Hansen *et al.* 2024). The carbonates commonly have a laminated texture and are also occasionally bioturbated (Fig. 3C). The mineralogical composition of both shales and carbonates is quartz, feldspar, phyllosilicates, calcite, dolomite, and ankerite. A semi-quantitative analysis reveals an increased amount of

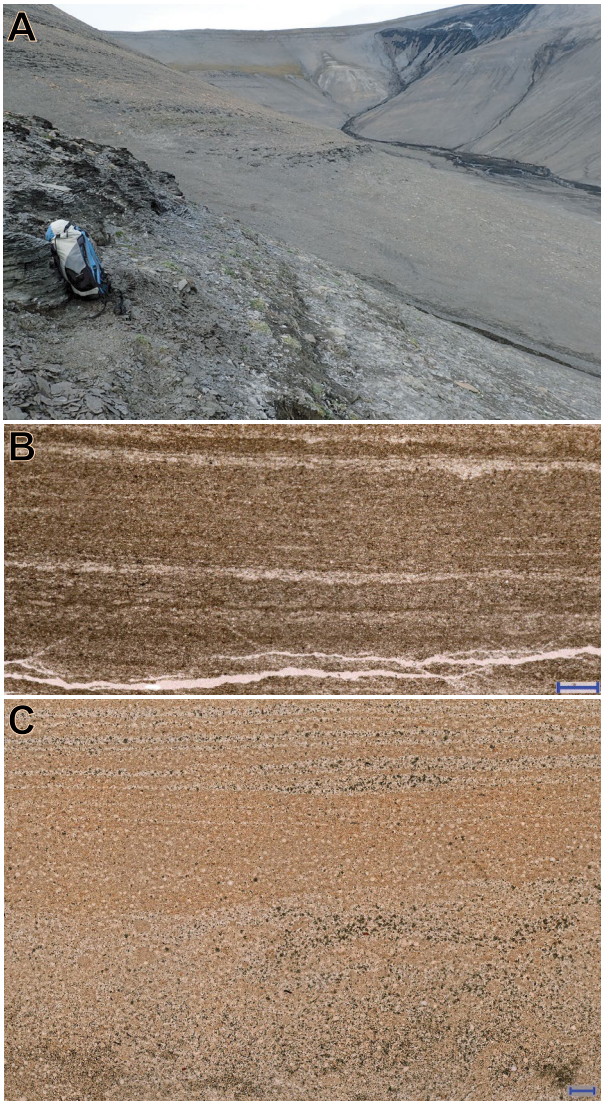

Fig. 3. A, transition from the Lusitaniadalen to the Vendomdalen Member at the Stensiöfjellet outcrop with the backpack placed on the SSB. B, STA 102 P shows the presence of numerous finely <1 mm thick layered structures. (blue scale: 1 mm). C, STC 4 shows shift from a bioturbated texture to a laminated texture. Thin section images (blue scale: 1 mm).

ankerite and dolomite in the Lusitaniadalen Member just below the hiatus (Supplementary Material Fig. 1).

The Vendomdalen Member is composed of fine-grained dark shale and intercalated carbonate nodule beds. Both shales and carbonate nodule have a laminated texture similar to the Lusitaniadalen Member and contain high amounts of pyrite. The mineralogical compositions of both lithologies in the Vendomdalen Member are similar to those in the Lusitaniadalen Member. The semi-quantitative analysis shows an increase in both pyrite and phyllosilicates and a decrease in feldspar content throughout the Vendomdalen Member towards the top of the section (Supplementary Material Fig. 1). Selected samples analysed for their clay mineralogy from both members were found to contain chlorite, illite, and mixed-layer clays.

RockEval Pyrolysis

Following the modified Van-Krevelen diagram (van Krevelen & Schuyer 1961) the shales of Stensiöfjellet data plot within the range of Kerogen Type II and III (Fig. 4 A). As the Hydrogen Index (HI) increases towards the top of the section, a trend from Type III to Type II is observed. The TOC content in the Lusitaniadalen Member is approximately 1 wt.% and increases to an average of 3 wt.% in the Vendomdalen Member. The T_{max} of all samples has a range between 426 °C and 442 °C. No trends in T_{max} values are observed.

Particulate organic matter composition

Particulate organic matter is marked by the presence of marine particles (homogenized sheets and flakes, acritarchs, green algae, algal clusters AOM, and foraminiferal test linings) and terrestrial particles (phytoclasts, cuticles, inertinite, membranes, spores, pollen grains, and fungal remains) throughout the studied succession. The main characteristic of the particulate organic matter (POM) is the presence of so-called homogenized sheets and flakes (sensu Vigran in Mørk *et al.* (1999)). POM from the Lusitaniadalen Member is marked by marine-terrestrial ratios of about 50%, whereas in the Vendomdalen Member the marine fraction increases to about 70%, mainly due to the higher relative abundance of homogenized sheets and flakes (supplementary Fig. 2). *Leiospheridia* spp. and fungal remains are slightly more abundant in the Lusitaniadalen Member and show an intermittent 'abundance peak' in the uppermost part of the Lusitaniadalen Member.

Elemental compositions

Titanium (Ti) and aluminium (Al) are regarded as proxies for detrital mineral input (Fig. 5). Titanium concentrations are decreasing throughout the section from about 150 ppm at the base to just above 50 ppm at the top. Aluminium concentrations are also decreasing towards the top of the section, with a higher variability close to the hiatus. The Chemical Index of Alteration (CIA) is a ratio for quantifying the degree of chemical weathering (Nesbitt & Young 1982).

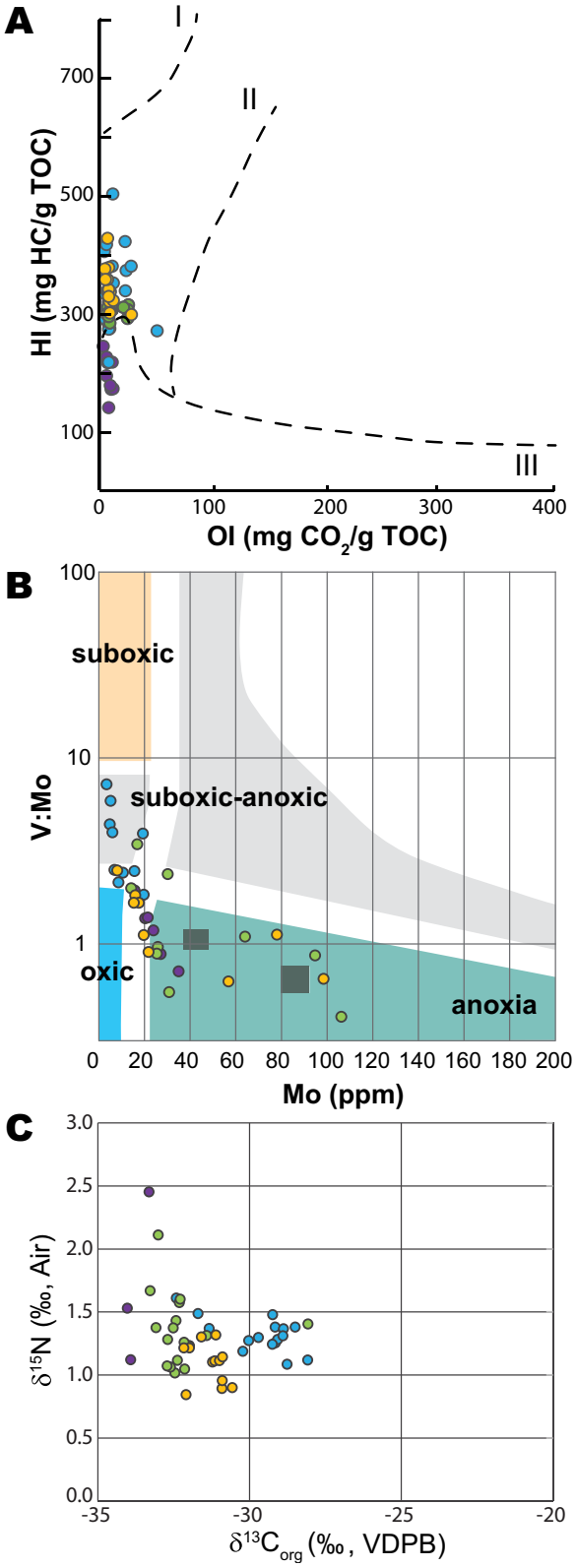

Fig. 4. Cross plots with colour coded data points following depth (see Figure 2). A, modified Van Krevelen Diagram. B, Mo vs V/Mo biplot following Piper and Calvert (2009) with dark teal squares in the anoxia field indicating values for the euxinic Black Sea and Cariaco Basin. C, $\delta^{13}C_{org\ bulk}$, versus $\delta^{15}N$ plot.

The results show rather variable values between 65 and 80 in the Lusitaniadalen Member and near the hiatus (Fig. 5). At the base of the Vendomdalen Member the CIA values are constant at around 75. Throughout the Vendomdalen Member, there are some small variations, but starting at 85 m the CIA values steadily decrease.

Thorium (Th) concentration can be used as a sedimentation rate proxy (e.g. Jarochowska *et al.* 2020). Th concentrations are variable in the Lusitaniadalen Member and have a range between 8 and 11.5 ppm (Fig. 5). In the Vendomdalen Member, Th concentrations average at a constant value of about 11.5 ppm. Zirconium and rubidium ratio (Zr/Rb) is a proxy used for determining grainsize with past studies showing robust results in Triassic of Spitsbergen (Dypvik & Harris 2001). The consolidated state of the sediment samples made it impossible to measure grainsize using more conventional methods. In the Lusitaniadalen Member the values remain high with an average of 2.4. In the first 10 m of the Vendomdalen Member values vary strongly between 1.5 and 2.1. Above 40 m the values are relatively consistent at around 1.5 (Fig. 5).

To gain a better understanding of changing redox conditions, the elemental proxies molybdenum versus vanadium/molybdenum biplot (Mo vs. V/Mo) (Piper & Calvert 2009) (Fig. 4B), uranium (U) and uranium normalized to sedimentation rate (U/Th) (Jones & Manning 1994) (Fig. 5) were used. The elements Mo, V and U were chosen as our preferred process tracers, as the poor correlation with elements such as, Ti and Al ($r< \pm 0.25$; Supplementary Material Fig. 3) that are commonly used as direct proxies of terrestrial provenance rather than process tracers. Hence Mo, V, and U appear not to be influenced by changes in terrestrial inputs. In the Mo vs. V/Mo biplot (Fig. 4B) large variation between the various phases of deposition can be recognized. Particularly between 28 and 46 m (blue interval) around the member boundary the samples have low Mo concentrations and intermediate V/Mo values. The purple interval of the Lusitaniadalen Member, as well as the green and yellow interval of the Vendomdalen Member has values trending towards higher Mo concentrations and lower V/Mo values. The green and yellow interval has larger variations. The U and U/Th start with values of 8 ppm and 0.8 at the base of the section (Fig. 5). They decrease at the hiatus to U values of 4 ppm and U/Th of 0.4. Thereafter values of both proxies increase throughout the Vendomdalen Member to U ≈ 11 ppm and a U/Th ratio of 1.2. Thorium, zirconium, rubidium and uranium content was measured by XRF while molybdenum and vanadium were measured with an ICP-OES.

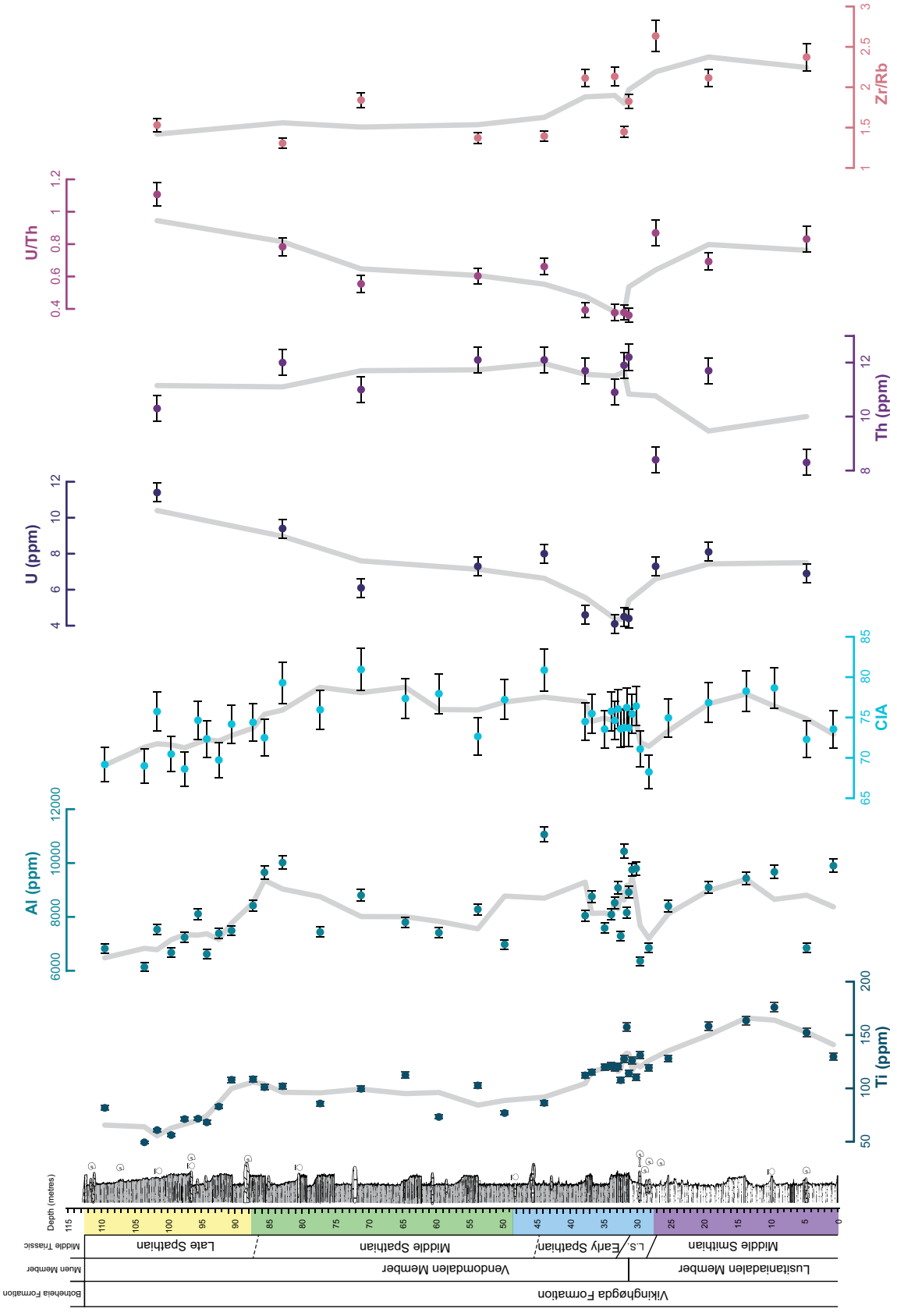

Fig. 5. The Stensiöfjellet section with formation, member boundaries and Lower Triassic substages. Variations of the Ti, Al, CIA (Chemical Index of Alteration), U, Th, U/Th ratio and Zr/Rb ratio at Stensiöfjellet section. The grey line in each diagram represents a 3-point moving average.

To assess nutrient fluctuations, the major nutrients phosphorus and nitrogen were analysed. Throughout the Lusitaniadalen Member, phosphorus (P) concentrations are constant at around 650 ppm (Fig. 2). At the top of the member just before the hiatus, the P concentrations increase to 909 ppm, remaining high with an average of 896 ppm within the basal 5 m of the Vendomdalen Member. Thereafter, the P decreases to approximately 677 ppm. Above 85 m, P content increases to a higher average, but concentrations are more heterogeneous. Total nitrogen content (TN) is below detection limit for most samples within the Lusitaniadalen Member, with only three samples having values of just below 0.1 wt.%. At the hiatus, the values increase to about 0.1 wt% and continue to increase throughout the Vendomdalen Member to 0.2 wt% (Fig. 2).

Carbon and nitrogen isotope compositions

In the Lusitaniadalen Member, the $\delta^{13}C_{org}$ values are rather constant averaging to a value of –33.5‰ up until approximately 29 m (Fig. 2). The $\delta^{13}C_{carb}$ values have more variability with a range between –7‰ and –2‰ within the Lusitaniadalen Member (Supplementary Material Fig. 4). At the transition between the Lusitaniadalen and Vendomdalen members, the $\delta^{13}C_{carb}$ and $\delta^{13}C_{org}$ values both change towards more positive values by about 5‰. This positive excursion begins in the topmost part of the Lusitaniadalen Member and peaks in the basal part of the Vendomdalen Member. The $\delta^{13}C_{org}$ peaks at –28.8‰ approximately 3.5 m above the hiatus. The $\delta^{13}C_{carb}$ peaks at –0.24‰, ca. 2.5 m above the hiatus. After the positive peak, the $\delta^{13}C_{carb}$ values are relatively constant at about –2‰. The $\delta^{13}C_{org}$ values gradually decrease to an average value of –32‰ between 45 and 86 m. At the top of the section above 86 m, the $\delta^{13}C_{org}$ values increase to –30‰ towards the top of the studied Stensiöfjellet section. The measured $\delta^{13}C_{carb}$ values show a different trend to the $\delta^{13}C_{org}$ values. The $\delta^{13}C_{carb}$ and $\delta^{13}C_{org}$ do not correlate for the given section ($R^2 = 0.29$; Supplementary Material Fig. 4). In $\delta^{13}C_{carb}$ and $\delta^{18}O$ cross plots the values plot within a range of values that are compatible with a meteoric water and hence diagenetic overprint (Supplementary Material Fig. 4). $\delta^{13}C_{carb}$ and the total inorganic carbon content also correlate (Supplementary Material Fig. 4). Therefore, the $\delta^{13}C_{carb}$ values are influenced by a later secondary meteoric water overprint and do not directly correspond to a primary signal that would allow for a palaeoenvironmental interpretation.

The nitrogen isotope compositions ($\delta^{15}N$) decrease from values of 2.5‰ to 1.5‰ throughout the Lusitaniadalen Member. In the Vendomdalen Member $\delta^{15}N$ values remain constant at an average of 1.2‰ (Fig. 2).

Discussion

Organic matter maturity and composition

Organic matter maturity and composition has been examined to determine the dominant organic carbon source. This information is fundamental for understanding organic carbon cycling and burial. It is also essential when using organic based proxies for palaeoenvironmental interpretations.

The thermal maturity of the Stensiöfjellet samples is constantly low with T_{max} values between 430 to 440 °C indicating a maturity at the base of the oil window (burial temperature < 100 °C). This is further supported by the palynomorph colour (TAS 4, Batten (1982)) and the conodont alteration index of 1–1.5 (Epstein *et al.* 1977; Leu *et al.* 2024) showing early mature conditions. This is lower than measured for other Lower Triassic Spitsbergen sections (Leith *et al.* 1993; Mørk *et al.* 1999). In southern Sassendalen, the Wallenbergfjellet section has a high thermal maturity (Hammer *et al.* 2019). This difference could be linked to less emplacement of Cretaceous sills or greater distance to these sills in northern Sassendalen compared to other locations in southern Sassendalen (Hammer *et al.* 2019).

As the thermal maturity is constant and low, the organic matter composition at Stensiöfjellet can confidently be interpreted as mixed marine-terrestrial (predominantly kerogen type III) in the Lusitaniadalen Member and a more marine organic matter composition (predominantly kerogen type II) in the Vendomdalen Member (Fig. 4 A). This interpretation is compatible with decreasing $\delta^{15}N$ values in the Lusitaniadalen Member as well as increasing HI values and POM composition throughout the entire section. This transition from largely terrestrial to more marine organic matter between the two members correlates with the increase in TOC (Fig. 2).

Carbon isotope excursion

The global positive $\delta^{13}C$ excursion has frequently been used as a marker for the SSB. However, there is inconsistency in the position of the SSB in relation to the $\delta^{13}C$ excursion. Some have placed the boundary at the onset of the positive excursion (Wignall *et al.* 2016), in the middle (Galfetti *et al.* 2007), whereas in other publications the SSB is placed exactly at the positive peak (Foster *et al.* 2017; Grasby *et al.* 2013).

The interpretation of a bulk $\delta^{13}C$ record can also be tricky due to overriding local effects skewing the curve.

At Stensiöfjellet an approximately 5‰ positive bulk organic carbon isotope excursion ($\delta^{13}C_{org}$) is present at the member boundary and the SSB (Fig. 2). This curve resembles the documented $\delta^{13}C_{org}$ record from Kongressfjellet, Festningen and Wallenbergfjellet in Svalbard (Galfetti *et al.* 2007; Hansen *et al.* 2024; Wignall *et al.* 2016) and other $\delta^{13}C$ records documented in the Tethys realm (e.g. Widmann *et al.* 2020, and references therein). The organic matter composition (see discussion in Organic Matter Maturity and Composition) and the $\delta^{13}C_{org}$ curve do not directly correlate and therefore the effect of the compositional change in organic matter is thought to be marginal to the overall change in the isotopic composition. However, it is likely that the change in organic matter composition above the member boundary to more marine-derived organic matter would also have an influence on the isotopic values. This would mean that the $\delta^{13}C_{org}$ values could have been controlled more closely by $\delta^{13}C_{DIC}$ values in the marine waters of the Vendomdalen Member rather than by the atmospheric CO_2 isotopic compositions taken up by the terrestrial organic matter in the Lusitaniadalen Member, contributing towards a more positive $\delta^{13}C_{org}$ value. In addition, the hiatus at the SBB has also led to a skewed $\delta^{13}C_{org}$ curve. Therefore, it cannot unequivocally be used to identify the placement of the SSB. Ammonoids and conodonts indicate the SSB to be placed within an interval of approximately 1.5 m around the member boundary Hansen *et al.* (2021, 2024), and Leu *et al.* (2024).

Sea level fluctuations

Transgression and regression cycles mark the Triassic depositional history of the Norwegian Barents Shelf (Mørk *et al.* 1989; Vigran *et al.* 2014). In the Triassic Barents Sea, shelf transgression and regression were controlled by tectonic subsidence and eustatic sea level fluctuations (Embry 1988; Glørstad-Clark *et al.* 2011; Haq 2018). On the continental shelf sea level fluctuations influence sedimentary working as well as sediment grainsize and composition. These will in turn influence organic carbon burial via the increased potential of remineralization through remobilization and organic matter mineral interactions. The Stensiöfjellet section in eastern Central Spitsbergen is more distal compared to other frequently studied sites such as the Festningen section due to the eastward-deepening trend seen in Lower Triassic deposits of Svalbard (Grasby *et al.* 2016a; Hammer *et al.* 2019; Mørk *et al.* 1982).

At Stensiöfjellet, gradually deeper marine conditions are noted throughout the Smithian and Spathian. This is seen firstly in the sedimentological change from a sandy shale in the Lusitaniadalen Member to a silty shale in the Vendomdalen Member. The change in grain size is also noted through the stepwise decrease of Zr/Rb ratios (Fig. 5). The decrease in Ti and Al contents throughout the section also reflects decreasing detrital, sand-sized mineral inputs with increasing clay-sized mineral inputs (Fig. 5). The presence of a Spitsbergen wide hiatus at the SSB (Mørk *et al.* 1999; Vigran *et al.* 2014) is in accordance with a sequence boundary. These changes are similar to those observed at Ledalen to the southwest (Hansen *et al.* 2018), as well as the earlier interpretations of the Vikinghøgda Formation, which is thought to have been deposited in successively deepening marine basins (Mørk *et al.* 1999). The hiatus at the member boundary observed throughout Svalbard (Mørk *et al.* 1999; Vigran *et al.* 2014) is another clear indication for sea level fluctuations influencing sedimentation. It encompasses a time span of two ammonoid zones, which is equivalent to approximately 250 kyr (Hansen *et al.* 2021; Widmann *et al.* 2020). It remains unclear if the hiatus originates due to non-deposition or erosion. It is plausible that a regression followed by a transgression occurred during this time interval, defining the hiatus. The regression could have originated from an eustatic decrease in sea level due to global cooling in the latest Smithian (Goudemand *et al.* 2019; Haq 2018). The subsequent transgression likely originated from further tectonic sinking of the basin (Glørstad-Clark *et al.* 2011) as well as sea level rise in the Spathian (Embry 1997).

At Stensiöfjellet it is likely that condensed horizons are present in the succession as indicated by ammonoid zones (Hansen *et al.* 2021, 2024; Leu *et al.* 2024). In the sandy shales of the Lusitaniadalen Member, Th concentrations change with the sedimentation rate (i.e. a decrease at 20 m) and Zr/Rb ratios change with grain size (Fig. 5). This suggests a shift from proximal to distal depositional settings. In a generally more proximal setting of the Lusitaniadalen Member the likelihood of sediment reworking, and the presence of hiatuses or condensed horizons is more marked. In the Vendomdalen Member, Th values remain high with a low sedimentation rate. Zr/Rb values decrease stepwise first around the hiatus and then about 7 m above this hiatus, supporting deposition of fine-grained sediments. At the Marmierfjellet section further to the west a nodular phosphate-rich bone bed has been described from the Vendomdalen Member

(Hansen *et al.* 2018). This has been interpreted as a condensed horizon suggesting a maximum transgression in the middle Spathian. At Stensiöfjellet no such bone bed or nodular phosphate rich bed has been found within the Vendomdalen Member. Hiatuses or condensed beds cannot be excluded or confirmed based on sedimentological observation or geochemical data within the Lusitaniadalen and Vendomdalen members at Stensiöfjellet.

The overall deepening trend correlates with a change in organic matter type, TOC increase and decrease in grain size (see discussion in Organic Matter Maturity and Composition). It can be hypothesized that these components are interlinked and that sea level fluctuations are to some extent controlling organic carbon burial. In the Lusitaniadalen Member the decrease in allochthonous terrestrial organic matter is likely due to an increasing distance to the source because of the overall transgression. The Vendomdalen Member contains high TOC values and is composed of a fine-grained lithology deposited in a distal continental shelf environment. Studies on modern sediments show that organic matter is frequently associated with fine-grained mineral particles via absorption referred to as organic matter-mineral interactions (Keil *et al.* 1994; Mayer 1993, 1994). Modern, organic carbon rich marine sediments are commonly mud banks consisting of fine-grained mineral particles located in offshore continental shelf regions (Bianchi *et al.* 2018). Indeed, organic matter-mineral interactions are shown to play a role in stabilizing organic matter even in the geological past (Kennedy *et al.* 2014; Kennedy *et al.* 2002; Kennedy & Wagner 2011). The observations of this study correlate with those of modern environments pointing towards the possible role organic matter-mineral interactions played in preserving organic carbon in the Lower Triassic deposits of Stensiöfjellet.

Oxic and anoxic conditions

The oxygenation conditions of the ocean in the Early Triassic and especially across the SSB have been a central topic of research (e.g. Grasby *et al.* 2013; Tian *et al.* 2014; Wignall *et al.* 2016). As the degradation of organic matter varies strongly between aerobic and anaerobic conditions, it is pivotal to the preservation of organic matter and therefore carbon sequestration (Demaison & Moore 1980). At Stensiöfjellet, the darker shales give a coherently higher TOC content for the Vendomdalen Member. This change brings up many questions, including if local redox conditions might have played a role in organic carbon sequestration.

In the first 28 m of the Lusitaniadalen Member, high U concentrations as well as the scatterplot of Mo vs. V/Mo (purple phase) are compatible with suboxic or anoxic conditions (Fig. 4B). Hansen *et al.* (2018) has argued for oxic conditions in the Lusitaniadalen Member in Ledalen, Wallenbergfjellet, and the Stensiöfjellet sections in Central Spitsbergen, based on handheld XRF measurements of the redox-sensitive elements including U, V, and Mo. The difference between this study and results of Hansen *et al.* (2018) is likely due to the sensitivity of the redox proxies used and their redox potential. In Arctic Canada Grasby *et al.* (2013) noted increasingly anoxic and euxinic conditions during the Middle and Late Smithian, time equivalent to the deposition of the Lusitaniadalen Member.

At Stensiöfjellet, approximately at the member boundary (28–59 m depth), encompassing the upper Smithian and lower Spathian, all geochemical redox proxies are pointing towards more oxygenated conditions. This aligns with the work of Hansen *et al.* (2018) on Central Spitsbergen sections. It could be hypothesized that the oxygenated conditions are linked to sea level fluctuations at the member boundary and SSB. These oxygenated conditions would not explain the increase in TOC measured at the base of the Vendomdalen Member. The presence of oxygenated conditions at the SSB contrasts with Wignall *et al.* (2016) where euxinic conditions were reported during this time interval for the Festningen and Vindodden sections in Spitsbergen. In Arctic Canada, an increase in oxygenated conditions has been noted across the SSB and in the lower Spathian, but still dysoxic conditions are thought to have prevailed (Grasby *et al.* 2013).

In the Vendomdalen Member above 59 m an increase in anoxia, possibly even reaching euxinia, is indicated by all redox proxies (Figs 4B, 5). It is, however, unclear when exactly and at what rate anoxia was established as U content and U/Th ratios indicate increasingly anoxic conditions at lower stratigraphic levels than Mo and V. The Mo vs. V/Mo biplot values from the Vendomdalen Member (green and yellow phase) also show larger redox variations (Fig. 4B). Hansen *et al.* (2018) also observed an increase in anoxia towards the top of the Vendomdalen Member, but noted differences between sections of Central Spitsbergen, where the Wallenbergfjellet sections indicate anoxic conditions closer to the SSB compared to Stensiöfjellet sections. The increase in anoxia and intermittent euxinia is observed in many Spathian successions across Svalbard (Grasby *et al.* 2020; Hammer *et al.* 2019; Krajewski 2013; Wesenlund *et al.* 2022; Wignall *et al.* 2016) and in the middle to upper Spathian of Arctic Canada (Grasby *et al.* 2013).

When comparing organic matter content with redox-sensitive element trends no clear correlation can be observed (Figs 2, 4C, 5). This includes the suboxic to anoxic conditions and low TOC levels in the Lusitaniadalen Member as well as the high TOC values and oxic conditions in the first 20 m of the Vendomdalen Member. Therefore, the change in organic carbon sequestration cannot exclusively be contributed to fluctuations in the measured redox conditions of this Smithian and Spathian succession.

Marine nutrient availability

Marine nutrient availability and therefore marine primary productivity during the Early Triassic are still hotly debated. Some have suggested high post-PTB marine primary productivity (e.g. Meyer *et al.* 2011; Schobben *et al.* 2020; Schobben *et al.* 2015) while others have argued for low marine primary productivity throughout the entire Early Triassic (e.g. Grasby *et al.* 2016b; Grasby *et al.* 2020; Knies *et al.* 2022; Müller *et al.* 2022; Winguth *et al.* 2015). Grasby *et al.* (2016b) and Grasby *et al.* (2020) have even suggested the presence of a 'nutrient gap' and thus suggested a bioproductivity crisis throughout the Early Triassic. Understanding marine nutrient cycling and its influence on marine primary productivity is of key importance due to its control of the biological carbon pump. The biological carbon pump is the flux of organic carbon (OC) from the surface ocean to the deep sea and is an essential part of the carbon cycle (Volk & Hoffert 1985).

At Stensiöfjellet an increase in both total nitrogen (TN) and total phosphorus (TP) occurs at the member boundary (Fig. 2). This increase has not been observed in past studies on more proximal sections such as Festningen in western Spitsbergen (Grasby *et al.* 2020). At Stensiöfjellet TN remains constant throughout the Vendomdalen Member. The N isotopic values only indicate a change in organic matter composition to more marine organic matter (see Organic Matter Maturity and Composition). The TP values increase particularly at the base and top of the Vendomdalen Member (Fig. 2). Phosphorus content in sediments is influenced by multiple factors such as sedimentation rate, redox conditions, and TP content in the water column, as well as the diagenetic conditions (Ruttenberg 2003). No parallels are seen between TP content and sedimentation rate estimated from Th concentrations (Fig. 5). Therefore, it is thought to be unlikely that fluctuations of TP are exclusively determined by a change in sedimentation rate. Parallels are, however, noted between TP and redox proxies (Figs 4C, 5). In the Vendomdalen Member as anoxia increases above 45 m (Figs 4C and 5), P content decreases (Fig. 2). Anoxia in the water column and at the sediment water interface would inhibit P remineralization and thus would allow it to be released and recycled within the water column (e.g. Van Cappellen & Ingall 1994; Van Cappellen & Ingall 1996) affecting the nutrient flux to the epipelagic marine environment. It is possible that this increase in TP and TN has not been recognized in other SSB sections (Grasby *et al.* 2020) due to the closer proximity to the shoreline leading to a longer hiatus at the SSB or to variable local conditions. In the overlying Middle Triassic Botneheia Formation TP content is known to increase substantially (Wesenlund *et al.* 2022).

In the Smithian and Spathian the increase in TP and TN content is possibly caused by a shift in marine nutrient cycling linked to an increased nutrient flux to the epipelagic marine environment during the Smithian–Spathian transition and hence an increase in the bioproductivity and export of organic carbon to the sediment. As such this increase in buried TOC at the SSB in the presence of oxic water conditions must be related to an increase in primary productivity. High rates of primary productivity could also have had an influence on increasing anoxic conditions towards the top of the Vendomdalen Member, which in turn would have inhibit P remineralization in the sediment allowing it to be released and recycled back into the water column maintaining high level of primary productivity and explaining the lower TP values of the middle Spathian.

We hypothesize that the phosphorus and nitrogen nutrient source is more likely to be of continental origin, rather than exclusively of a marine, upwelling origin, for example. This is based on: (1) the palaeogeographical situation, where a gently sloping ramp (Mørk *et al.* 1999) is an unlikely location for upwelling; (2) the carbon and nitrogen isotope cross plot that does not show an upwelling signal (low $\delta^{13}C$ values; Fig. 4 C); and (3) Al content and CIA values support an increased influx of weathered continental material in continental weathering around the member boundary, which could have influenced a nutrient flux to the marine system.

Conclusions

This study presents a detailed multiproxy approach to understand local to regional palaeoenvironmental variability and its influence on sedimentary organic carbon sequestration from the middle Smithian to the late Spathian in northern Sassendalen, Central Spitsbergen. The following can be concluded:

1. The increase of TP and TN concentrations at the SSB point to a shift in local marine nutrient cycling, which likely led to an increase in local marine primary productivity. An increase in marine primary productivity related to a higher terrestrial nutrient influx of P and N, led to changes in the biological carbon pump increasing organic carbon burial, which is observed in increasing TOC values in the Spathian. The change in TP throughout the section is, in part, likely also linked to changing bottom water redox conditions observed in redox sensitive element concentrations.
2. All geochemical redox proxies indicate dysoxic to anoxic conditions in the middle Smithian and increasing anoxia in the middle and late Spathian. Oxic conditions are present at the SSB. The middle Smithian marine bottom water anoxic conditions have however no obvious correlation to sedimentary organic carbon sequestration. In the middle and late Spathian increasing anoxia and high TOC values imply that anoxia likely had an influence on sedimentary organic carbon sequestration.
3. The correlation between an increase in TOC and increased abundance of fine-grained mineral components in the Vendomdalen Member implies that organic matter mineral interaction played a role in the preservation of organic matter and likely increasing organic carbon sequestration. This aligns with findings from studies on modern organic matter rich sediments and black shales from the geological past (cf. Kennedy *et al.* 2002).
4. The organic matter composition at Stensiöfjellet shows a low thermal maturity throughout the section, unlike other locations in Spitsbergen (Hammer *et al.* 2019; Leith *et al.* 1993). As such this section is suited for further organic geochemical studies to gain deeper insights into organic carbon cycling during the Smithian and Spathian.

Acknowledgements.– This work is supported by the Swiss National Science Foundation (Project n° SNF 200020_160055 to H.B., T.V. and CRSII5-180253 to H.B., T.V., Urs Schaltegger, Maura Brunetti). Borhan Bagherpour is thanked for sample preparation. Thank you to S. Grasby and an anonymous reviewer for their helpful comments. Thank you to the Svalbard Research Council for granting field work permits (RiS ID 10772).

Supplementary Information

Supplementary material Fig. 1. The Stensiöfjellet section with formation, member boundaries and Lower Triassic substages. Semi-quantitative mineralogical XRD data of all identified minerals from Stensiöfjellet in weight percent (wt. %).

Supplementary material Fig. 2. Particulate organic matter Stensiöfjellet A. E = Euflemmingites float, A = Arctoceras, J = Juvenites, W = Wasatchites, B = Bajarunia (STC), K = Keyserlingites, S = Svalbardiceras, P, S Popovites, Svalbardiceras (STC).

Supplementary material Fig. 3. Correlation plot of all ICP-OES elemental concentrations with Pearson coefficient.

Supplementary material Fig. 4. The Stensiöfjellet section with formation, member boundaries and Lower Triassic substages following the biostratigraphy of Leu *et al.* 2024. The colour code across the depth scale bar is also used in cross plots to the right. Variations of $\delta^{13}C_{carb}$, total inorganic carbon (TIC, wt. %), $\delta^{18}O$, and $\delta^{13}C_{org, bulk}$. The grey line in the depth plot represents a 3-point moving average.

Supplementary material Raw Data. Table containing Stensiöfjellet geochemical data from manuscript

References

Adatte, T., Stinnesbeck, W., Keller, G., Ryder, G., Fastovsky, D. & Gartner, S. 1996: Lithostratigraphic and mineralogic correlations of near K/T boundary clastic sediments in northeastern Mexico: implications for origin and nature of deposition. *Geological Society America Special Papers 307*, 211–226 https://doi.org/10.1130/0-8137-2307-8.211

Aspila, K.I., Agemian, H. & Chau, A.S.Y. 1976: A semi-automated method for the determination of inorganic, organic and total phosphate in sediments. *Analyst 101*, 187–197 https://doi.org/10.1039/AN9760100187

Batten, D. 1982: Palynofacies, palaeoenvironments and petroleum. *Journal of Micropalaeontology 1*, 107–114 https://doi.org/10.1144/jm.1.1.107

Batten, D., Grenfell, H., Jansonius, J. & McGregor, D. 1996: Green and blue-green algae. *Palynology: Principles and Applications 36*, 205–214

Bianchi, T.S., Cui, X., Blair, N.E., Burdige, D.J., Eglinton, T.I. & Galy, V. 2018: Centers of organic carbon burial and oxidation at the land-ocean interface. *Organic Geochemistry 115*, 138–155 https://doi.org/10.1016/j.orggeochem.2017.09.008

Brayard, A. & Bucher, H. 2015: Permian-Triassic extinctions and rediversifications, *Ammonoid Paleobiology: From Macroevolution to Paleogeography*, 465–473. Springer, Doordrecht. https://doi.org/10.1007/978-94-017-9633-0

Brühwiler, T., Bucher, H., Brayard, A. & Goudemand, N. 2010: High-resolution biochronology and diversity dynamics of the Early Triassic ammonoid recovery: the Smithian faunas of the Northern Indian Margin. *Palaeogeography, Palaeoclimatology, Palaeoecology 297*, 491–501 https://doi.org/10.1016/j.palaeo.2010.09.001

Demaison, G.J. & Moore, G.T. 1980: Anoxic environments and oil source bed genesis. *Organic Geochemistry 2*, 9–31 https://doi.org/10.1016/0146-6380(80)90017-0

Dypvik, H. & Harris, N.B. 2001: Geochemical facies analysis of fine-grained siliciclastics using Th/U, Zr/Rb and (Zr+Rb)/Sr ratios. *Chemical Geology 181*, 131–146 https://doi.org/10.1016/S0009-2541(01)00278-9

Embry, A.F. 1988: Triassic Sea-Level Changes: Evidence from the Canadian Arctic Archipelago. *In:* Wilgus, C. K., Hastings, B.S., Posamentier, H., Wagoner, J.V., Ross, C.A. & Kendall, C.G.S.C., eds, *Sea-Level Changes: An Integrated Approach*, 249–259 SEPM Society for Sedimentary Geology, SEPM Society for Sedimentary Geology, https://doi.org/10.2110/pec.88.01.0249

Embry, A.F. 1997: Global sequence boundaries of the Triassic and their identification in the Western Canada Sedimentary Basin. *Bulletin of Canadian Petroleum Geology 45*, 415–433 https://doi.org/10.35767/gscpgbull.45.4.415

Epstein, A.G., Epstein, J.B. & Harris, L.D. 1977: Conodont color alteration – an index to organic metamorphism. *Geological Survey Professional Paper 995* https://doi.org/10.3133/pp995

Espitalie, J., Deroo, G. & Marquis, F. 1986: La pyrolyse Rock-Eval et ses applications. Troisième partie. *Revue de l'Institut français du Pétrole 41*, 73–89 https://doi.org/10.2516/ogst:1986003

Foster, W.J., Danise, S., Price, G.D. & Twitchett, R.J. 2017: Subsequent biotic crises delayed marine recovery following the late Permian mass extinction event in northern Italy. *PLoS One 12*, e0172321 https://doi.org/10.1371/journal.pone.0172321

Galfetti, T., Hochuli, P.A., Brayard, A., Bucher, H., Weissert, H. & Vigran, J.O. 2007: Smithian-Spathian boundary event: Evidence for global climatic change in the wake of the end-Permian biotic crisis. *Geology 35*, 291–294 https://doi.org/10.1130/G23117A.1

Glørstad-Clark, E., Birkeland, E.P., Nystuen, J.P., Faleide, J.I.& Midtkandal, I. 2011: Triassic platform-margin deltas in the western Barents Sea. *Marine and Petroleum Geology 28*, 1294–1314 https://doi.org/10.1016/j.marpetgeo.2011.03.006

Goudemand, N., Romano, C., Leu, M., Bucher, H., Trotter, J.A. & Williams, I.S. 2019: Dynamic interplay between climate and marine biodiversity upheavals during the Early Triassic Smithian-Spathian biotic crisis. *Earth-Science Reviews 195*, 169–178 https://doi.org/10.1016/j.earscirev.2019.01.013

Grasby, S., Beauchamp, B., Embry, A. & Sanei, H. 2013: Recurrent early Triassic ocean anoxia. *Geology 41*, 175–178 https://doi.org/10.1130/G33599.1

Grasby, S.E., Beauchamp, B., Bond, D.P.G., Wignall, P.B. & Sanei, H. 2016a: Mercury anomalies associated with three extinction events (Capitanian Crisis, Latest Permian Extinction and the Smithian/Spathian Extinction) in NW Pangea. *Geological Magazine 153*, 285–297 https://doi.org/10.1017/S0016756815000436

Grasby, S.E., Beauchamp, B. & Knies, J. 2016b: Early Triassic productivity crises delayed recovery from world's worst mass extinction. *Geology 44*, 779–782 https://doi.org/10.1130/g38141.1

Grasby, S.E., Knies, J., Beauchamp, B., Bond, D.P., Wignall, P. & Sun, Y. 2020: Global warming leads to Early Triassic nutrient stress across northern Pangea. *Geological Society of America Bulletin 132*, 943–954 https://doi.org/10.1130/B32036.1

Hammer, Ø., Jones, M.T., Schneebeli-Hermann, E., Hansen, B.B. & Bucher, H. 2019: Are Early Triassic extinction events associated with mercury anomalies? A reassessment of the Smithian/Spathian boundary extinction. *Earth-Science Reviews 195*, 179–190 https://doi.org/10.1016/j.earscirev.2019.04.016

Hansen, B.B., Hammer, Ø. & Nakrem, H.A. 2018: Stratigraphy and age of the Grippia niveau bonebed, Lower Triassic Vikinghøgda formation, Spitsbergen. *Norsk Geologisk Tidsskrift 98*, 175–187 https://dx.doi.org/10.17850/njg98-2-02

Hansen, B.B., Bucher, H., Schneebeli-Hermann, E. & Hammer, Ø. 2021: The middle Smithian (Early Triassic) ammonoid Arctoceras blomstrandi: conch morphology and ornamentation in relation to stratigraphy. *Papers in Palaeontology 7*, 1435–1457 https://doi.org/10.1002/spp2.1348

Hansen, B.B., Bucher, H.F.R., Schneebeli-Hermann, E. & Hammer, Ø. 2024: Smithian and Spathian paleoecological records of the Vikinghøgda Formation in Central Spitsbergen. *Lethaia,* 1–15 https://doi.org/10.18261/let.57.1.3

Haq, B.U. 2018: Triassic eustatic variations re-examined. *Geological Society of America Today 28*, 4–9 https://doi.org/10.1130/GSATG381A.1

Hautmann, M., Bagherpour, B., Brosse, M., Frisk, Å., Hofmann, R., Baud, A., Nützel, A., Goudemand, N. & Bucher, H. 2015: Competition in slow motion: the unusual case of benthic marine communities in the wake of the end-P ermian mass extinction. *Palaeontology 58*, 871–901 https://doi.org/10.1111/pala.12186

Hermann, E., Hochuli, P.A., Bucher, H., Brühwiler, T., Hautmann, M., Ware, D. & Roohi, G. 2011a: Terrestrial ecosystems on North Gondwana following the end-Permian mass extinction. *Gondwana Research 20*, 630–637 https://doi.org/10.1016/j.gr.2011.01.008

Hermann, E., Hochuli, P.A., Méhay, S., Bucher, H., Brühwiler, T., Ware, D., Hautmann, M., Roohi, G., ur-Rehman, K. & Yaseen, A. 2011b: Organic matter and palaeoenvironmental signals during the Early Triassic biotic recovery: The Salt Range and Surghar Range records. *Sedimentary Geology 234*, 19–41 https://doi.org/10.1016/j.sedgeo.2010.11.003

Hochuli, P., Colin, J. & Vigran, J.O. Triassic biostratigraphy of the Barents Sea area, *In Proceedings Correlation in Hydrocarbon Exploration: Proceedings of the conference Correlation in Hydrocarbon Exploration organized by the Norwegian Petroleum Society Bergen, Norway, 3–5 October 1989*, 131–153. Springer, Doordrecht. https://doi.org/10.1007/978-94-009-1149-9_12

Jarochowska, E., Nohl, T., Grohganz, M., Hohmann, N., Vandenbroucke, T.R.A. & Munnecke, A. 2020: Reconstructing depositional rates and their effect on paleoenvironmental proxies: the case of the Lau Carbon Isotope Excursion in Gotland, Sweden. *Paleoceanography and Paleoclimatology 35*, e2020PA003979 https://doi.org/10.1029/2020PA003979

Jones, B. & Manning, D.A.C. 1994: Comparison of geochemical indices used for the interpretation of palaeoredox conditions in ancient mudstones. *Chemical Geology 111*, 111–129 https://doi.org/10.1016/0009-2541(94)90085-X

Keil, R.G., Tsamakis, E., Fuh, C.B., Giddings, J.C. & Hedges, J.I. 1994: Mineralogical and textural controls on the organic composition of coastal marine sediments: Hydrodynamic separation using SPLITT-fractionation. *Geochimica et Cosmochimica Acta 58*, 879–893 https://doi.org/10.1016/0016-7037(94)90512-6

Kennedy, M.J., Löhr, S.C., Fraser, S.A. & Baruch, E.T. 2014: Direct evidence for organic carbon preservation as clay-organic nanocomposites in a Devonian black shale; from deposition to diagenesis. *Earth and Planetary Science Letters 388*, 59–70 https://doi.org/10.1016/j.epsl.2013.11.044

Kennedy, M.J., Pevear, D.R. & Hill, R.J. 2002: Mineral surface control of organic carbon in black shale. *Science 295*, 657–660 https://doi.org/10.1126/science.1066611

Kennedy, M.J. & Wagner, T. 2011: Clay mineral continental amplifier for marine carbon sequestration in a greenhouse ocean. *Proceedings of the National Academy of Sciences 108*, 9776–9781 https://doi.org/10.1073/pnas.1018670108

Knies, J., Schönenberger, J., Zwingmann, H., van der Lelij, R., Smelror, M., Vullum, P.E., Brönner, M., Vogt, C., Fredin, O. & Müller, A. 2022: Continental weathering and recovery from ocean nutrient stress during the Early Triassic Biotic Crisis. *Communications Earth & Environment 3*, 1–12 https://doi.org/10.1038/s43247-022-00480-z

Krajewski, K.P. 2013: Organic matter–apatite–pyrite relationships in the Botneheia Formation (Middle Triassic) of eastern Svalbard: relevance to the formation of petroleum source rocks in the NW Barents Sea shelf. *Marine and Petroleum Geology 45*, 69–105 https://doi.org/10.1016/j.marpetgeo.2013.04.016

Kübler, B. 1983: Dosage quantitatif des minéraux majeurs des roches sédimentaires par diffraction X. *Cahiers de l'Institut de Géologie Series AX*, 1–13

Leith, T., Weiss, H., Mørk, A., Elvebakk, G., Embry, A., Brooks, P., Stewart, K., Pchelina, T., Bro, E. & Verba, M. 1993: Mesozoic hydrocarbon source-rocks of the Arctic region, *Norwegian Petroleum Society Special Publications 2* Elsevier, Elsevier, 1–25 https://doi.org/10.1016/B978-0-444-88943-0.50006-X

Leu, M., Schneebeli-Hermann, E., Hansen, B.B., Hammer, Ø., Lindemann, F.-J. & Bucher, H. 2024: Spatiotemporal dynamics of nektonic biodiversity and vegetation shifts during the Smithian -Spathian transition: conodont and palynomorph insights from Svalbard *Lethaia 57* (2). https://doi.org/10.18261/let.57.2.3

Luz, Z.A.S. 2022: *Characterizing Conodont Bioapatite from the Early Triassic: an Analytical and Palaeoclimatological Approach*. Unpublished Ph.D. thesis, University of Lausanne, 154 p.

McLennan, S.M. 1993: Weathering and Global Denudation. *The Journal of Geology 101*, 295–303 https://doi.org/10.1086/648222

Mayer, L.M. 1993: Organic Matter at the Sediment-Water Interface, *in* Engel, M. H. and Macko, S. A., eds, *Organic Geochemistry: Principles and Applications*, 171–184. Springer, Boston, https://doi.org/10.1007/978-1-4615-2890-6_7

Mayer, L.M. 1994: Surface area control of organic carbon accumulation in continental shelf sediments. *Geochimica et Cosmochimica Acta 58*, 1271–1284 https://doi.org/10.1016/0016-7037(94)90381-6

Meyer, K.M., Yu, M., Jost, A.B., Kelley, B.M. & Payne, J.L. 2011: δ13C evidence that high primary productivity delayed recovery from end-Permian mass extinction. *Earth and Planetary Science Letters 302*, 378–384 https://doi.org/10.1016/j.epsl.2010.12.033

Mørk, A., Elvebakk, G., Forsberg, A.W., Hounslow, M.W., Nakrem, H.A., Vigran, J.O. & Weitschat, W. 1999: The type section of the Vikinghogda Formation: a new Lower Triassic unit in central and eastern Svalbard. *Polar Research 18*, 51–82 https://doi.org/10.3402/polar.v18i1.6558

Mørk, A., Embry, A.F. & Weitschat, W. 1989: Triassic transgressive-regressive cycles in the Sverdrup Basin, Svalbard and the Barents Shelf, 113–130. Springer, Dordrecht. https://doi.org/10.1007/978-94-009-1149-9_11

Mørk, A., Knarud, R. & Worsley, D. Depositional and diagenetic environments of the Triassic and Lower Jurassic succession of Svalbard. *In: Proceedings Arctic Geology and Geophysics: Proceedings of the Third International Symposium on Arctic Geology, Calgary, Alberta, Canada, 1982*, Volume Memoir 8, Canadian Society of Petroleum Geologist, 371–398

Müller, J., Sun, Y.D., Yang, F. & Joachimski, M. 2022: Phosphorus cycle and primary productivity changes in the Tethys Ocean during the Permian-Triassic transition: Starving marine ecosystems. *Frontiers in Earth Science 10*, 286 https://doi.org/10.3389/feart.2022.832308

Nagul, E.A., McKelvie, I.D., Worsfold, P. & Kolev, S.D. 2015: The molybdenum blue reaction for the determination of orthophosphate revisited: opening the black box. *Analytica Chimica Acta 890*, 60–82 https://doi.org/10.1016/j.aca.2015.07.030

Nesbitt, H. & Young, G. 1982: Early Proterozoic climates and plate motions inferred from major element chemistry of lutites. *Nature 299*, 715–717 https://doi.org/10.1038/299715a0

Orchard, M.J. 2007: Conodont diversity and evolution through the latest Permian and Early Triassic upheavals. *Palaeogeography, Palaeoclimatology, Palaeoecology 252*, 93–117 https://doi.org/10.1016/j.palaeo.2006.11.037

Payne, J.L., Lehrmann, D.J., Wei, J., Orchard, M.J., Schrag, D.P. & Knoll, A.H. 2004: Large perturbations of the carbon cycle during recovery from the end-Permian extinction. *Science 305*, 506–509 https://doi.org/10.1126/science.1097023

Piper, D.Z. & Calvert, S.E. 2009: A marine biogeochemical perspective on black shale deposition. *Earth-Science Reviews 95*, 63–96. https://doi.org/10.1016/j.earscirev.2009.03.001

Romano, C., Goudemand, N., Vennemann, T.W., Ware, D., Schneebeli-Hermann, E., Hochuli, P.A., Brühwiler, T., Brinkmann, W. & Bucher, H. 2013: Climatic and biotic upheavals following the end-Permian mass extinction. *Nature Geoscience 6*, 57–60 https://doi.org/10.1038/ngeo1667

Ruttenberg, K.C. 2003: The Global Phosphorus Cycle. *In:* Holland, H.D. & Turekian, K.K., (eds), *Treatise on Geochemistry*, 585–643. Pergamon, Oxford, https://doi.org/10.1016/B0-08-043751-6/08153-6

Schobben, M., Foster, W.J., Sleveland, A., Zuchuat, V., Svensen, H.H., Planke, S., Bond, D.P., Marcelis, F., Newton, R.J. & Wignall, P.B. 2020: A nutrient control on marine anoxia during the end-Permian mass extinction. *Nature Geoscience 13*, 640–646 https://doi.org/10.1038/s41561-020-0622-1

Schobben, M., Stebbins, A., Ghaderi, A., Strauss, H., Korn, D. & Korte, C. 2015: Flourishing ocean drives the end-Permian marine mass extinction. *Proceedings of the National Academy of Sciences 112*, 10298–10303 https://doi.org/10.1073/pnas.1503755112

Spötl, C. & Vennemann, T.W. 2003: Continuous-flow isotope ratio mass spectrometric analysis of carbonate minerals. *Rapid Communications in Mass Spectrometry 17*, 1004–1006 https://doi.org/10.1002/rcm.1010

Stanley, S.M. 2009: Evidence from ammonoids and conodonts for multiple Early Triassic mass extinctions. *Proceedings of the National Academy of Sciences 106*, 15264–15267 https://doi.org/10.1073/pnas.0907992106

Tian, L., Tong, J., Algeo, T.J., Song, H., Song, H., Chu, D., Shi, L. & Bottjer, D.J. 2014: Reconstruction of Early Triassic ocean redox conditions based on framboidal pyrite from the Nanpanjiang Basin, South China. *Palaeogeography, Palaeoclimatology, Palaeoecology 412*, 68–79 https://doi.org/10.1016/j.palaeo.2014.07.018

Traverse, A. 2007: *Paleopalynology*, Springer Dordrecht. https://doi.org/10.1007/978-1-4020-5610-9

Tyson, R.V. 1995: *Sedimentary Organic Matter: Organic Facies and Palynofacies*, Chapman & Hall, London, https://doi.org/10.1007/978-94-011-0739-6

Van Cappellen, P. & Ingall, E.D. 1994: Benthic phosphorus regeneration, net primary production, and ocean anoxia: A model of the coupled marine biogeochemical cycles of carbon and phosphorus. *Paleoceanography 9*, 677–692 https://doi.org/10.1029/94PA01455

Van Cappellen, P. & Ingall, E.D. 1996: Redox stabilization of the atmosphere and oceans by phosphorus-limited marine productivity. *Science 271*, 493–496 https://doi.org/10.1126/science.271.5248.493

van Krevelen, D. & Schuyer, J. 1961: *Coal Science: An introduction to Chemistry of Coal*, Elsevier, Amsterdam.

Vérard, C. 2019: Panalesis: towards global synthetic palaeogeographies using integration and coupling of manifold models. *Geological Magazine 156*, 320–330 https://doi.org/10.1017/S0016756817001042

Vigran, J.O., Mangerud, G., Mørk, A., Worsley, D. & Hochuli, P.A. 2014: *Palynology and Geology of the Triassic Succession of Svalbard and the Barents Sea*, Norges geologiske undersokelse, https://doi.org/10.5167/UZH-99116

Volk, T. & Hoffert, M.I. 1985: Ocean Carbon Pumps: Analysis of Relative Strengths and Efficiencies in Ocean-Driven Atmospheric CO2 Changes, *The Carbon Cycle and Atmospheric CO2: Natural Variations Archean to Present*, 99–110 https://doi.org/10.1029/GM032p0099

Wesenlund, F., Grundvåg, S.-A., Engelschiøn, V.S., Thießen, O. & Pedersen, J.H. 2022: Multi-elemental chemostratigraphy of Triassic mudstones in eastern Svalbard: implications for source rock formation in front of the world's largest delta plain. *The Depositional Record 8*, 718–753 https://doi.org/10.1002/dep2.182

Widmann, P., Bucher, H., Leu, M., Vennemann, T., Bagherpour, B., Schneebeli-Hermann, E., Goudemand, N. & Schaltegger, U. 2020: Dynamics of the largest carbon isotope excursion during the Early Triassic biotic recovery. *Frontiers in Earth Science 8*, 196 https://doi.org/10.3389/feart.2020.00196

Wignall, P.B., Bond, D.P., Sun, Y., Grasby, S.E., Beauchamp, B., Joachimski, M.M. & Blomeier, D.P. 2016: Ultra-shallow-marine anoxia in an Early Triassic shallow-marine clastic ramp (Spitsbergen) and the suppression of benthic radiation. *Geological Magazine 153*, 316–331 https://doi.org/10.1017/S0016756815000588

Winguth, A.M.E., Shields, C.A. and Winguth, C. 2015: Transition into a Hothouse World at the Permian–Triassic boundary — a model study. *Palaeogeography, Palaeoclimatology, Palaeoecology 440*, 316–327. https://doi.org/10.1016/j.palaeo.2015.09.008

Zhang, L., Orchard, M.J., Brayard, A., Algeo, T.J., Zhao, L., Chen, Z.-Q. & Lyu, Z. 2019: The Smithian/Spathian boundary (late Early Triassic): A review of ammonoid, conodont, and carbon-isotopic criteria. *Earth-Science Reviews 195*, 7–36 https://doi.org/10.1016/j.earscirev.2019.02.014